Available online at www.sciencedirect.com
ScienceDirect
Ceramics International 36 (2010) 1289–1296
CERAMICS INTERNATIONAL
www.elsevier.com/locate/ceramint

Coarsening, coalescence and sintering of hexagonal ZnO elongated nanoparticles

I-Hsien Liu, Pouyan Shen *

Department of Materials and Optoelectronic Science, National Sun Yat-sen University, Kaohsiung, Taiwan, ROC

Received 24 September 2009; received in revised form 18 November 2009; accepted 28 December 2009
Available online 1 February 2010

Abstract

The pore size distribution coupled with N_2 adsorption–desorption hysteresis isotherm and the change of specific surface area were studied in the temperature range of 600–900 °C for hexagonal ZnO nanoparticles. Cylindrical pores are characteristic of the dry pressed ZnO nanoparticles with elongated shape (aspect ratio 2–3) and well-developed $\{0\,1\,\bar{1}\,0\}$ and (0 0 0 1) surfaces, and hence not a good indicator of subsequent coarsening/coalescence and/or sintering events. On the other hand, the vigorous onset coarsening, coalescence and then sintering of the elongated nanoparticles was satisfactorily differentiated to occur within minutes having apparent activation energy of 39 ± 7, 47 ± 4, and 55 ± 5 kJ/mol based on $t_{0.3}$, $t_{0.5}$ and $t_{0.7}$, i.e. time for 30, 50 and 70% surface area reduction, respectively. The proposition of coarsening/coalescence processes being differentiable from a later sintering process by specific activation energies is in accord with the increase and then decrease of the average pore size. The minimum temperature for $\{0\,1\,\bar{1}\,0\}$ and (0 0 0 1)-specific coarsening/coalescence of the nanorods is 516 °C based on the extrapolation of steady specific surface area reduction rates to null.

Keywords: A. Firing; A. Powders; B. Surfaces; B. Porosity; D. ZnO

1. Introduction

It is a general belief that melting point decreases considerably with size reduction under the influence of capillarity effect as proved by in situ transmission electron microscopic observations of semiconductor nanocrystals [1]. Having a lower melting point, finer sized particles are expected to show fair sinterability at relatively low temperatures because of a relatively high homologous temperature (T/T_m, where T_m is melting point). A pronounced coarsening and repacking process of oxide nanoparticles was suggested to occur for effective sintering before reaching 60% relative density based on the densification curves of CeO_2 and Y_2O_3 in the temperature range 600–1500 °C (cf. Fig. 7 of Ref. [2]).

Recently, the pore size distribution coupled with N_2 adsorption–desorption hysteresis isotherm and the change of specific surface area have been successfully used to study the onset coarsening/coalescence kinetics of oxide nanoparticles such as γ-Al_2O_3 with equiaxed shape [3], and $Co(OH)_2$-derived CoO with plate-like shape [4]. The microstructural observations of the samples subjected to early stage firing within similar temperature range [3,4] not only supports a pronounced coarsening and repacking process of oxide nanoparticles proposed by Chen and Chen [2] but also shed light on the phase behavior of relevant oxide nanocondensates produced in a dynamic pulsed laser ablation (PLA) process [5]. The H1 type adsorption–desorption hysteresis of the type IV according to the International Union of Pure and Applied Chemistry (IUPAC) scheme [6] appeared to be good indicator of cylindrical pores formation and hence an onset coarsening/coalescence process for equiaxed ceramic particles in a specified temperature range [3,4]. This H1 type based indication of onset coarsening/coalescence process however may be invalid for compact nanorods already with cylindrical pores before firing.

Here, wurtzite-type (W–)ZnO nanoparticles of semiconducting and piezoelectric importance [7] were chosen to show that cylindrical pores are indeed characteristic of the dry pressed nanoparticles with elongated shape (aspect ratio 2–3) and well-developed polar and nonpolar surfaces, and hence not a good indicator of subsequent coarsening/coalescence

* Corresponding author. Tel.: +886 7 5254060; fax: +886 7 5254099.
E-mail address: pshen@mail.nsysu.edu.tw (P. Shen).

0272-8842/$36.00
doi:10.1016/j.ceramint.2009.12.022

events upon static firing. The surface area reduction rate was however, satisfactorily used to differentiate the vigorous coarsening, coalescence and sintering processes with specific activation energy in the so-called early sintering stage. The minimum temperature for such processes is also inferred by extrapolating the steady specific surface area reduction rates to null.

2. Experimental

Powdery W–ZnO (Aldrich) less than 100 nm in particle diameter was die-pressed at 650 MPa into disks ca. 5 mm in diameter and 2 mm in thickness. The powders were dispersed on a carbon-coated collodion film for phase, shape and size distribution characterizations using transmission electron microscopy (TEM, JEOL3010 at 300 kV) coupled with bright field image (BFI), lattice image and selected area electron diffraction (SAED) techniques. Such dry pressed powders were used for isothermal firing in the temperature range of 600–900 °C for specified time period up to 1 h in an open air furnace. Microstructure changes of the samples due to dry pressing and heating were studied by scanning electron microscopy (SEM, JEOL 6330 at 20 kV) using secondary electron image (SEI) mode. The phase identity of the dry pressed and heated samples was also determined by X-ray diffraction (XRD, Cu Kα, 40 kV, 30 mA at 0.05° and 3 s per step).

Nitrogen adsorption/desorption isotherms of the dry pressed and then heated powders were conducted at liquid nitrogen temperature of 77 K using a Micromeritics ASAP 2020 instrument. The surface area and pore size distributions were obtained from the N_2 adsorption and desorption branch, using the Brunauer–Emmett–Teller (BET) method [8] and Barrett–Joyner–Halenda (BJH) method [9], respectively. The BET isotherm and BJH adsorption/desorption hysteresis type of the samples are classified according to the scheme of IUPAC [6]. The H1 type adsorption/desorption hysteresis loop of the type IV isotherm [6] was used as an indicator of cylindrical pore formation upon dry pressing of the elongated ZnO nanoparticles.

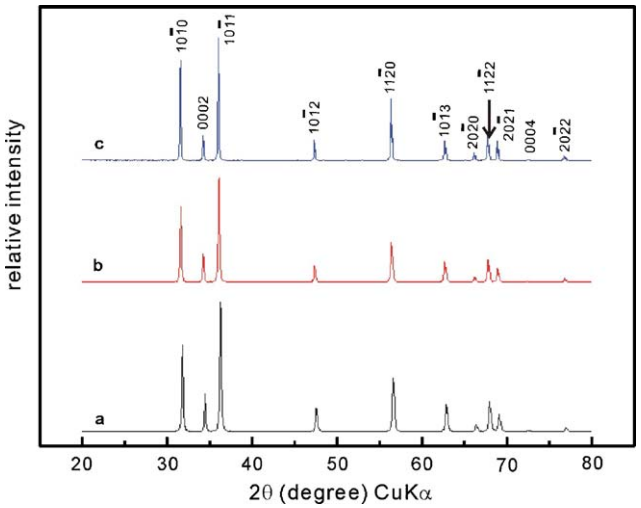

Fig. 1. XRD traces of ZnO powders: (a) dry pressed, (b) and (c) followed by static firing at 900 °C for 3 and 9 min, respectively showing no significant preferred orientation.

3. Results

3.1. Shape of the starting powders

The representative XRD traces of W–ZnO powders, either dry pressed or followed by static firing at 900 °C for 3 and 9 min (Fig. 1a–c), showed no preferred orientation in contrast to the ZnO condensates with preferred orientation $\{1\,0\,\bar{1}\,1\}$ when deposited on glass substrate by pulse laser ablation on Zn target in the presence of oxygen [5]. (Such an artificial epitaxy depends on the well-developed $\{1\,0\,\bar{1}\,1\}$ surfaces of the condensates, which enabled $\{1\,0\,\bar{1}\,1\}$-specific coalescence to form twin and single crystal [5].)

TEM BFI (Fig. 2a) and corresponding SAED pattern (Fig. 2b) showed that the starting ZnO powders are predominantly 50–70 nm in size with hexagonal rod shape yet in random orientation as indicated by ring diffractions indexed according to wurtzite-type structure. Fig. 3a and b

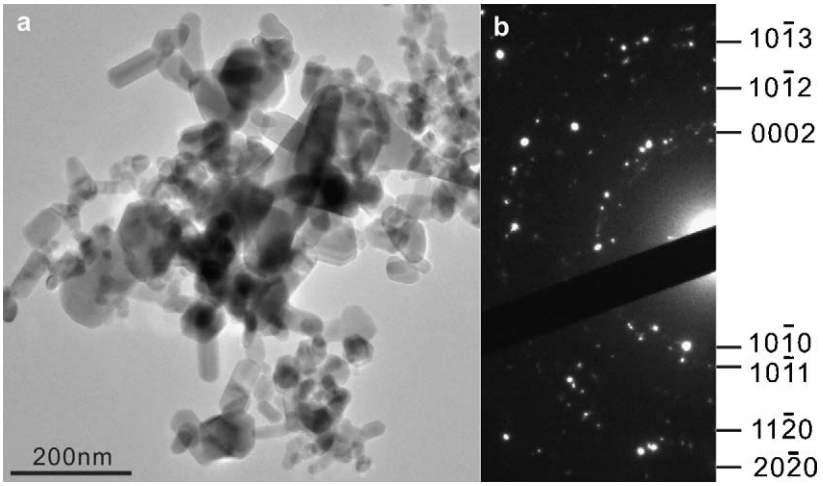

Fig. 2. TEM (a) BFI and (b) SAED of nano to submicron-sized ZnO powders with hexagonal rod shape in random orientation as indicated by ring diffractions indexed according to wurtzite-type structure.

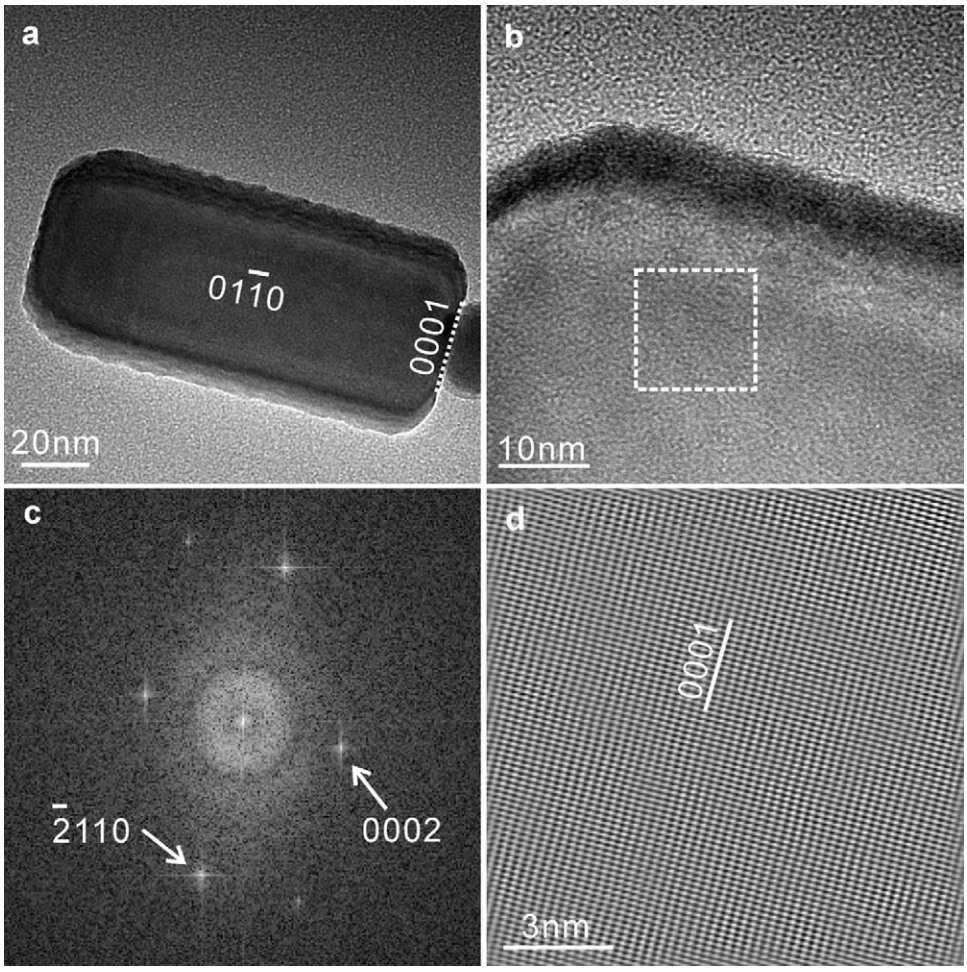

Fig. 3. TEM (a) BFI and (b) lattice image of an elongated ZnO nanoparticle with well-developed $(0\,1\,\bar{1}\,0)$ surface in top view and $(0\,0\,0\,1)$ surface edge on in $[0\,1\,\bar{1}\,0]$ zone axis, (c) and (d) 2D forward and inverse Fourier transform, respectively from the square region in (b) showing slightly corrugated $(0\,0\,0\,1)$ planes yet with no dislocation. It is the same as in Fig. 2.

showed further the BFI and lattice image of a representative ZnO nanoparticle with elongated shape and well-developed $(0\,1\,\bar{1}\,0)$ nonpolar surface and $(0\,0\,0\,1)$ polar surface. (Note $(0\,0\,0\,1)$ polar surface was also found in ZnO nanocondensates for $(h\,k\,i\,l)$-specific coalescence in a dynamic PLA process [5].) The 2D forward and inverse Fourier transform (Fig. 3b and c) showed the slightly corrugated $(0\,0\,0\,1)$ planes yet with no dislocation. The hexagonal ZnO nanoparticle showed another polar surface, i.e. $(\bar{1}\,1\,0\,1)$ facet, and again corrugated $(0\,0\,0\,1)$ planes in $[1\,1\,\bar{2}\,0]$ zone axis (not shown). (Note $(\bar{1}\,1\,0\,1)$ polar surface was also found in ZnO nanocondensates for $(h\,k\,i\,l)$-specific coalescence in a dynamic PLA process [5] and for subsequent growth of whiskers upon aging at 600 °C [10].) Still, such elongated nanoparticles tend to be attached on their better-developed lateral $(0\,1\,\bar{1}\,0)$ surfaces (not shown).

3.2. SEM observations of dry pressed and further heated samples

SEM observations indicated that dry pressing caused cylindrical pores among the elongated nanoparticles attached preferentially on their well-developed $(0\,1\,\bar{1}\,0)$ nonpolar surface, yet no appreciable cracking and particle size change (Fig. 4). The compact nanoparticles subjected to firing for almost half reduction of specific surface area showed repacking of the coarsened particles besides possibly further developed cylindrical pores as represented by the samples fired at 600 °C for 15 min (Fig. 5a), and 900 °C for 3 min (Fig. 5b).

By contrast, the samples subjected to longer firing time for almost 70% reduction of specific surface area in this temperature range showed various size of isolated pores presumably via various extent of grain-boundary diffusion to fill the pores among the significantly coarsened and hence equiaxed grains with triple junctions characteristic of solid-state sintering in the late firing stage (Fig. 6). Note the present ZnO nanoparticles did develop into whiskers despite prolonged firing up to 1 h at 600–900 °C. By contrast, isothermal (600 °C) atmospheric annealing of the ZnO/Zn composite deposit with preferred orientation $\{1\,0\,\bar{1}\,1\}_{ZnO}$ and $(0\,0\,0\,1)_{Zn}$, respectively on glass substrate caused self-catalyzed vapor–liquid–solid (VLS) growth of rod-like ZnO whiskers with unusual habit [10] or even tapered by an unusual VLS growth taking advantage of bottom molten source [11].

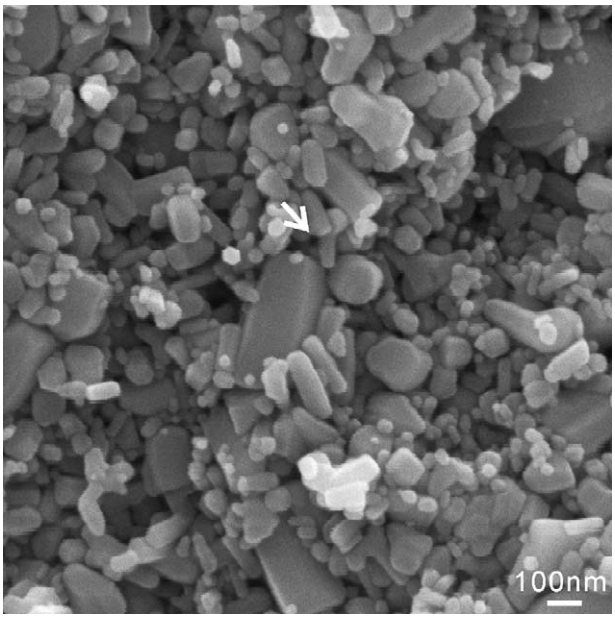

Fig. 4. SEM (SEI) image of the dry pressed ZnO nanoparticles showing dark dots (arrow) which could be the outcrops of cylindrical pores among the elongated nanoparticles.

3.3. Specific surface area, pore and microstructure changes upon heating

The BJH N_2 adsorption–desorption hysteresis isotherms for the elongated ZnO nanoparticles dry pressed and further fired at 600, 700, 800 and 900 °C for specified time periods are shown in Fig. 7a–d, respectively. The green body consisting of such sized powders shows a H1 type loop in the relative pressure range 0.85–1.0, which is characteristic of cylindrical pore [6]. The H1 type loop improves, presumably due to repacking of the nano-sized powders as discussed later, and shifts to a higher relative pressure (0.9–1.0) for the samples fired for ca. 10 min at 600 °C (Fig. 7a) and for a shorter time (<3 min) at higher temperatures (Fig. 7b–d). A longer firing time in this temperature range deteriorates the H1 type loop due to the change of cylindrical pores to isolated pores further shifting to a higher relative pressure (0.95–1.0) with various size and shape as indicated by the samples fired beyond 50 min at 600 °C (Fig. 7a), 20 min at 700 °C (Fig. 7b), 10 min at 800 °C (Fig. 7c) and 6 min at 900 °C (Fig. 7d).

BET data of the fired samples indicated that the specific surface area decreases whereas average pore size increases with the increase of dwelling time at a specific firing temperature for the elongated ZnO powders as compiled in Fig. 8. The drastic change of specific surface area and average pore size are related to the formation of cylindrical and/or truncated pores as revealed by the BJH analyses. The observed rate curves, i.e. the isothermal reduction of specific surface area versus time, are shown in Fig. 8a–d for the ZnO nanoparticles fired at 600–900 °C, respectively. The time $t_{0.5}$, i.e. with 50% reduction of specific surface area, as well as $t_{0.3}$ and $t_{0.7}$ were used for activation energy estimation and hence the differentiation of the underlying processes in various firing stages as discussed later.

4. Discussion

4.1. Adsorption–desorption hysteresis loop characteristic of cylindrical mesopores

Capillary condensation typically occurs for mesopores in a size range 2–50 nm to show type IV isotherm, which can be classified into H1 to H4 subtypes [6]. According to the present observations of BJH N_2 adsorption–desorption isotherms, the dry pressed ZnO nanoparticles via degassing before BET/BJH measurements have a H1 type hysteresis loop similar to the case of other mesoporous materials with a pore width range 2–50 nm [6]. Thus, H1 type based indication of onset coarsening/coalescence process is invalid for the present compact nanoparticles already with cylindrical pores before firing. The deterioration and shifting of the H1 type loop to a higher relative pressure, however, is good indication of the change of cylindrical pores into isolated pores in the later firing stage

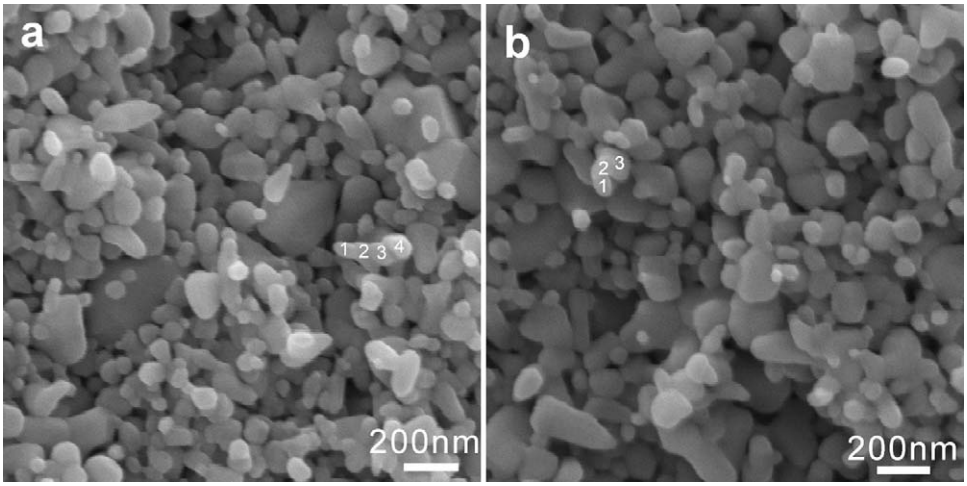

Fig. 5. Representative SEM (SEI) images of dry pressed ZnO powders subjected to firing at (a) 600 °C for 15 min and (b) 900 °C for 3 min to show repacking of the coarsened particles as numbered (cf. text).

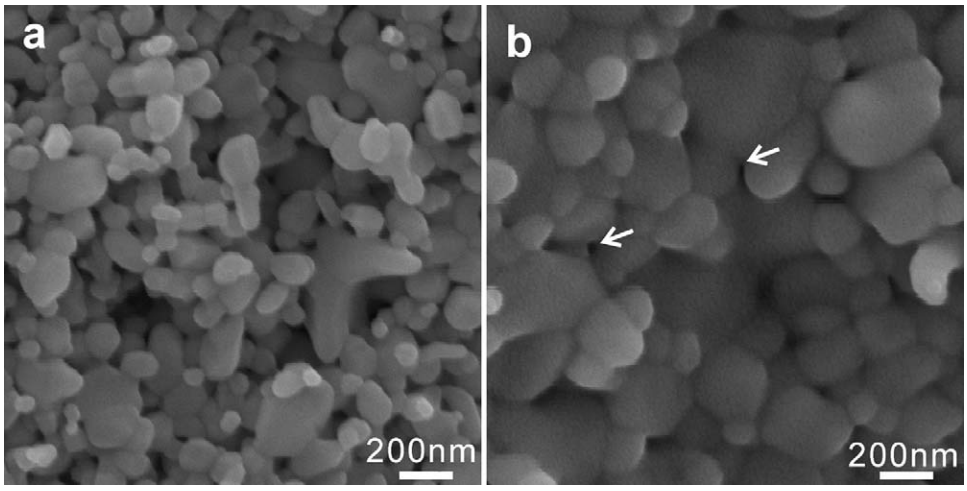

Fig. 6. Representative SEM (SEI) images of dry pressed ZnO powders subjected to firing at (a) 600 °C for 50 min and (b) 900 °C for 9 min, for more than 70% reduction of specific surface area via grain-boundary diffusion to fill in various extent the isolated pores (arrows) among the significantly coarsened and hence equiaxed grains in the late firing stage (cf. text).

involving more pronounced sintering as indicated by sample shrinkage by 15% coupled with more than 70% specific surface area change after firing at 900 °C for 9 min. The cylindrical pores among the elongated ZnO nanoparticles tended to coalesce for a larger average pore size in the early firing stage until sintering took place to decrease the pore size which is too small to detect, in particular when fired at higher temperatures. By contrast, the dry pressed CoO nanoplates derived from

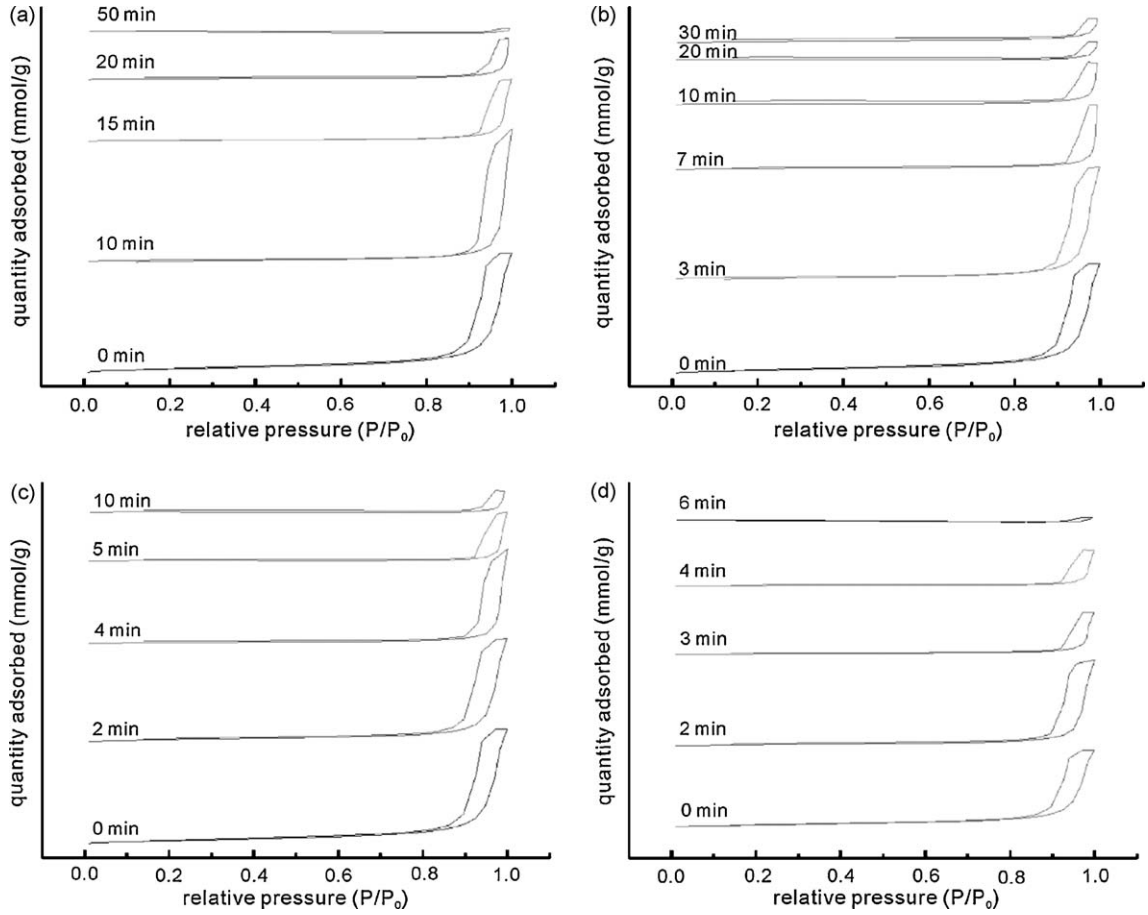

Fig. 7. BJH N_2 adsorption–desorption hysteresis isotherms for the dry pressed ZnO nanoparticles fired at various conditions: (a) 600 °C for 0–50 min, (b) 700 °C for 0–30 min, (c) 800 °C for 0–10 min, and (d) 900 °C for 0–6 min.

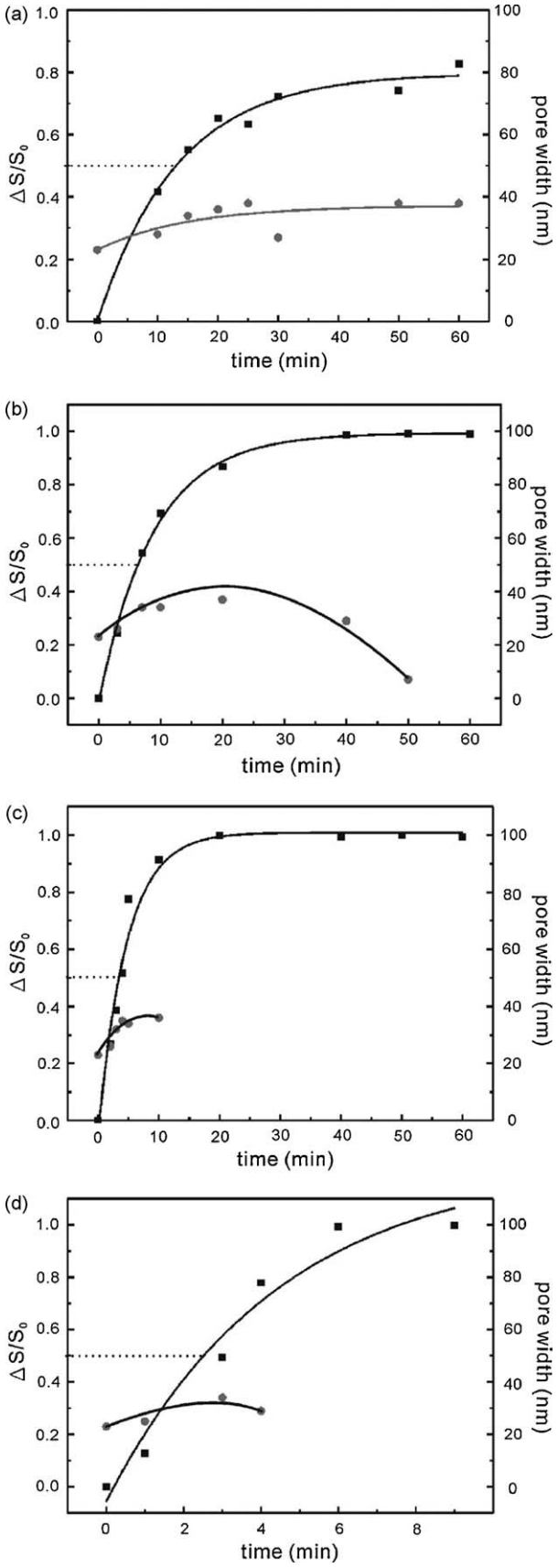

Fig. 8. Observed rate curves in terms of the reduction of specific surface area ($\Delta S/S_0$, where S_0 is the initial quantity, square symbol) and desorption pore size (circles) versus time for nanosize ZnO powder at (a) 600 °C, (b) 700 °C, (c) 800 °C and (d) 900 °C. The time $t_{0.5}$, i.e. with 50% reduction of specific surface area as denoted by dashed line as well as $t_{0.3}$ and $t_{0.7}$ (not denoted) were used for activation energy estimation in various firing stages for the nano-sized powders.

$Co(OH)_2$ do not have cylindrical pores for coalescence and therefore the pore size decreases rather than increases in the early firing stage [4].

4.2. Activation energy and mechanism of specific surface area change

On the basis of the rate curves (Fig. 8), the onset time $t_{0.5}$ for the elongated ZnO nanoparticles to decrease the specific surface area by 50% was determined as 15 ± 2, 7 ± 1, 4 ± 0.33, 3 ± 0.1 min at 600, 700, 800 and 900 °C, respectively. The corresponding Arrhenius plot of the reciprocal time $t_{0.5}$ for onset coarsening-coalescence versus the reciprocal temperature in Kelvin gives an apparent activation energy 47 ± 4 kJ/mol considering the maximum uncertainty of each data point (Fig. 9). As a comparison, the activation energies are 39 ± 7 and 55 ± 5 kJ/mol, based on $t_{0.3}$ and $t_{0.7}$, respectively. (According to BET data, $t_{0.3}$ is 6 ± 1.5, 3 ± 0.5, 2 ± 0.3, 1.5 ± 0.1 min at 600, 700, 800 and 900 °C, respectively; whereas $t_{0.7}$ is 28 ± 5, 11 ± 2, 6 ± 0.8, 4 ± 0.5 min at 600, 700, 800 and 900 °C, respectively.) We suggest that the activation energy difference can be rationalized by the sequential dominance of coarsening, coalescence and sintering processes in nascent, steady and later firing stages. The underlying mechanism would be surface diffusion, Brownian motion and grain-boundary diffusion of the nanorods for the coarsening, coalescence and sintering process, respectively. Repacking of coarsened nanorods is expected to occur only in the early firing stage. The proposition of coarsening/coalescence processes being differentiable from a later sintering process by specific activation energies is in accord with the pore size increase and then decrease of the elongated ZnO nanoparticles as mentioned.

The above activation energies with specified underlying mechanisms are reasonably compatible to that based on density measurements [12]. The activation energy of coarsening is 39 ± 7 kJ/mol for the present elongated ZnO nanoparticles 50–70 nm in size, whereas 20 kJ/mol for the equiaxed ZnO powder less than 40 nm in size [12]. A higher activation energy of coarsening for the present elongated ZnO nanoparticles can be rationalized by a larger particle size and $\{0\,1\,\bar{1}\,0\}$-specific growth and coalescence, although in much less extent than the case of $(h\,k\,i\,l)$-specific twinning whisker growth via vapor–liquid–solid (VLS) mechanism [10]. The ZnO whiskers were reported to extend along the zone axes of the well-developed polar surfaces $\{1\,0\,\bar{1}\,1\}$ for a beneficial lower electrostatic energy and surface energy, or via $\{1\,1\,\bar{2}\,1\}$-specific growth twinning and/or coalescence twinning for a beneficial fair coincidence-site lattice at the twin boundary [10]. The Zn particulates overlaid with ZnO nanocondensates having nearly orthogonal $\{1\,0\,\bar{1}\,1\}$ and $\{1\,1\,\bar{2}\,1\}$ facets were further found to self-catalyze unusual tapered W–ZnO whiskers upon isothermal atmospheric annealing, i.e. thermal oxidation, at 600 °C

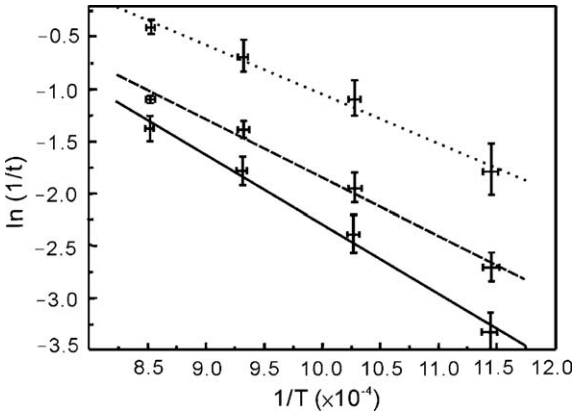

Fig. 9. Arrhenius plots of the logarithmic reciprocal time $t_{0.3}$ (dotted line), $t_{0.5}$ (dashed line) and $t_{0.7}$ (solid line) against reciprocal temperature (in Kelvin) for specific surface area decrease by 30, 50 and 70% with an activation energy of 39 ± 7, 47 ± 4 and 55 ± 5 kJ/mol, respectively from the dry pressed ZnO nanoparticles.

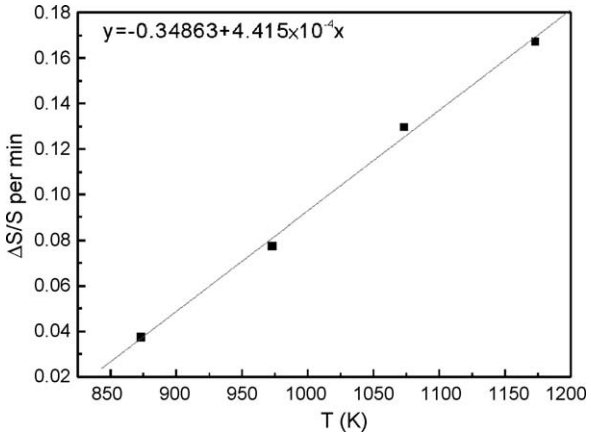

Fig. 10. Temperature dependent specific surface area reduction rate.

[11]. The tapered whiskers were rationalized by an alternative VLS growth, i.e. $\{1\,0\,\bar{1}\,1\}$ and $\{2\,\bar{1}\,\bar{1}\,1\}$-specific coalescence twinning growth from the ZnO condensates taking advantage of a partially molten bottom source of Zn and the adsorption of atoms at the whisker tips and ledges under the influence of capillarity effect [11]. The absence of whiskers in the present samples can be attributed to a larger particle size of the elongated ZnO nanoparticles and hence a melting/sublimation temperature too high to conduct a VLS growth.

The activation energy of sintering is 55 ± 5 kJ/mol for the present elongated ZnO nanoparticles, yet much higher (275 kJ/mol) for ZnO powders with bimodal particle size ca. 70 nm and micrometers when fired to 95–98% theoretical density [12]. A lower activation energy of sintering in the present case can be accounted for by a smaller particle size and hence a higher melting point, i.e. easier grain-boundary diffusion for a solid-state sintering process.

As for the activation energy of coalescence determined by $t_{0.5}$ in the steady state, it would more or less involve the attachment of well-developed nonpolar $\{0\,1\,\bar{1}\,0\}$ surface and minor polar (0 0 0 1) surface of the elongated ZnO nanoparticles. In fact, a maximum 180° rotation is able to unify the bicrystals undergoing $\{0\,1\,\bar{1}\,0\}$-specific attachment, whereas a maximum 60° is enough for (0 0 0 1)-specific unification analogous to the case of unifying the $Co(OH)_2$-derived hexagonal plate of CoO powders via (0 0 0 1) contact plane [4].

4.3. Engineering implications

W–ZnO, as an important semiconducting and piezoelectric material [7], has been tailored as various novel nanostructures by thermal evaporation because of its polar surfaces, which have nontransferable ionic charges arranged in such a configuration to minimize the electrostatic energy [13]. The polar surfaces are usually $\pm(0\,0\,0\,1)$, but occasionally $\pm\{0\,\bar{1}\,1\,1\}$ as observed in a nanohelical structure of W–ZnO [14]. According to recent high-resolution TEM and simulation [15], the oxygen-terminated $(0\,0\,0\,\bar{1})$ polar surface is flat, whereas Zn-terminated (0 0 0 1) polar surface appears to have Zn vacancies and outward displacement of Zn ions. The oxygen-terminated $(0\,\bar{1}\,1\,1)$ polar surface has two groups of oxygen ion positions; whereas Zn-terminated $(0\,1\,\bar{1}\,\bar{1})$ polar surface was not observed presumably due to its higher surface energy [15]. Regarding the interest of fabricating W–ZnO polycrystals for semiconducting and piezoelectric applications, the minimum temperature for $\{0\,1\,\bar{1}\,0\}$ and (0 0 0 1)-specific coarsening/coalescence of the elongated ZnO nanoparticles is determined as 789 K (516 °C) based on the extrapolation of steady specific surface area reduction rates, i.e. that measured at $t_{0.5}$, to null (Fig. 10). This minimum temperature may be extended to the case of W–ZnO nanocondensates in a dynamic process such as that under the effect of radiant heating via PLA [5]. (Laser ablation condensation is an effective method of producing W–ZnO nanoparticles more or less in agglomeration and coalescence due to the considerable associated heating effect [5].)

5. Conclusions

1. Cylindrical pores are characteristic of the dry pressed W–ZnO nanoparticles with elongated shape and well-developed $\{0\,1\,\bar{1}\,0\}$ and (0 0 0 1) surfaces, and hence not a good indicator of subsequent coarsening/coalescence and/or sintering events.
2. The vigorous onset coarsening, coalescence and then sintering of the elongated nanoparticles was satisfactorily differentiated to occur within minutes having apparent activation energy of 39 ± 7, 47 ± 4, and 55 ± 5 kJ/mol based on 30, 50 and 70% surface area reduction, respectively in the temperature range of 600–900 °C.
3. The proposition of coarsening/coalescence processes being differentiable from a later sintering process by specific activation energies is in accord with the increase and then decrease of the pore size.
4. The minimum temperature for $\{0\,1\,\bar{1}\,0\}$ and (0 0 0 1)-specific coarsening/coalescence of the nanorods is 516 °C based on the extrapolation of steady specific surface area reduction rates to null. This supports our previous supposition that W–ZnO particles in an assembly of

nanochain aggregates are able to coalesce and/or sinter into a close packed manner by radiant heating below 1000 °C in a dynamic laser ablation process.

Acknowledgments

Supported by Center for Nanoscience and Nanotechnology at NSYSU and National Science Council, Taiwan, ROC. We thank an anonymous referee for constructive comments.

References

[1] A.N. Goldstein, C.M. Echer, A.P. Alivisatos, Melting in semiconductor nanocrystals, Science 256 (1992) 1425–1427.
[2] P.L. Chen, I.W. Chen, Sintering of fine oxide powders, J. Am. Ceram. Soc. 80 (1997) 637–645.
[3] I.L. Liu, P. Shen, Onset coarsening-coalescence kinetics of γ-type related Al_2O_3 nanoparticles: implications to their assembly in a laser ablation process, J. Eur. Ceram. Soc. 29 (2009) 2235–2248.
[4] Y. Yeh, I.H. Liu, P. Shen, Onset coarsening/coalescence of cobalt oxides in the form of nanoplates vs. equi-axed micron particles, J. Eur. Ceram. Soc. 30 (2010) 677–688.
[5] B.H. Huang, P. Shen, S.Y. Chen, $\{1\,0\,\bar{1}\,1\}$ artificial epitaxy of dense ZnO on glass via pulse laser deposition, J. Eur. Ceram. Soc. 28 (2008) 2545–2555.
[6] K.S.W. Sing, D.H. Everett, R.A.W. Haul, L. Moscou, R.A. Pierotti, J. Rouquerol, T. Siemieniewska, Reporting physisorption data for gas/solid systems with special reference to the determination of surface area and porosity, Pure Appl. Chem. 57 (1985) 603–619.
[7] V.A. Coleman, C. Jagadish, in: C. Jagadish, S.J. Pearton (Eds.), Basic Properties and Applications of ZnO, in Zinc Oxide Bulk, Thin Films and Nanostructures, Elsevier, Oxford, 2006, p. 12.
[8] S. Brunauer, P.H. Emmett, E. Teller, Adsorption of gases in multimolecular layers, J. Am. Chem. Soc. 60 (1938) 309–319.
[9] E.P. Barrett, L.G. Joyner, P.P. Halenda, The determination of pore volume and area distribution in porous substances. I. Computations from nitrogen isotherms, J. Am. Chem. Soc. 73 (1951) 373–380.
[10] B.H. Huang, S.Y. Chen, P. Shen, $\{1\,0\,\bar{1}\,1\}$ and $\{1\,1\,\bar{2}\,1\}$-specific growth and twinning of ZnO whiskers, J. Phys. Chem. C 112 (2008) 1064–1071.
[11] B.H. Huang, P. Shen, S.Y. Chen, Tapered ZnO whiskers: $\{h\,k\,i\,l\}$-specific mosaic twinning VLS growth from a partially molten bottom source, Nanoscale Res. Lett. 4 (2009) 503–512.
[12] A.P. Hynes, R.H. Doremus, E.W. Siegel, Sintering and characterization of nanophase zinc oxide, J. Am. Ceram. Soc. 85 (2002) 1979–1987.
[13] Z.L. Wang, X.Y. Kong, Y. Ding, P. Gao, W.L. Hughes, R. Yang, Y. Zhang, Semiconducting and piezoelectric oxide nanostructures induced by polar surfaces, Adv. Funct. Mater. 14 (2004) 943–956.
[14] R. Yang, Y. Ding, Z.L. Wang, Deformation-free single-crystal nanohelixes of polar nanowires, Nano Lett. 4 (2004) 1309–1312.
[15] Y. Ding, Z.L. Wang, Profile imaging of reconstructed polar and non-polar surfaces of ZnO, Surf. Sci. 601 (2007) 425–433.